Communication

Mechanical Behavior of Three-Dimensional Braided Nickel-Based Superalloys Synthesized *via* Pack Cementation

NICOLAS LIPPITZ, DINC ERDENIZ, KEITH W. SHARP, and DAVID C. DUNAND

Braided tubes of Ni-based superalloys are fabricated *via* three-dimensional (3-D) braiding of ductile Ni-20Cr (wt pct) wires followed by post-textile gas-phase alloying with Al and Ti to create, after homogenization and aging, γ/γ' strengthened lightweight, porous structures. Tensile tests reveal an increase in strength by 100 MPa compared to as-braided Ni-20Cr (wt pct). An interrupted tensile test, combined with X-ray tomographic scans between each step, sheds light on the failure behavior of the braided superalloy tubes.

https://doi.org/10.1007/s11661-018-4467-9

Due to their low density and high surface area, porous metals are of interest for many thermostructural applications.[1–6] Use of three-dimensional (3-D) weaving and 3-D braiding technologies makes it possible to produce periodic cellular materials from metal wires with specifically tailored properties.[7–14] For applications at elevated temperatures, *e.g.*, in the aerospace industry, properties, such as creep, oxidation, and corrosion resistance, are required. Nickel-based superalloys are well suited for such applications, but, as weaving and braiding require ductile materials to sustain high bending angles, commercial nickel-based superalloy wires cannot be used for this purpose. Hence, in this study, we decouple the braiding and alloying steps by using ductile Ni-20Cr (all compositions are given in weight percent) wires for 3-D braiding and subsequently alloying them using pack cementation, a chemical vapor deposition process. A multistep heat treatment, consisting of transient liquid phase (TLP) bonding, homogenizing, solutionizing, and aging, is used to form bonds between adjacent wires and to achieve a braided structure made from γ'-strengthened wires with a near uniform composition and microstructure. This process was previously demonstrated for 3-D woven structures[8,15] and microlattices.[16] In this study, it is applied to braided tubes, examining the microstructure development as well as mechanical properties. In addition to monotonous tensile tests, an interrupted tensile test in combination with X-ray tomography is used to analyze the failure behavior of the superalloy braided tubes.

Three-dimensional braiding produces a wire (fiber) architecture, where the thickness is equivalent to several layers of a traditional two-dimensional braid and each individual wire can traverse the full thickness of the part. The braided tubes used in this study were fabricated from Ni-20Cr wires with a diameter of 202 μm using a rotary braiding technique described in Reference 8. Each braid contained 160 wires and the final tubular structure had an outer diameter of ~ 6 mm and an inner diameter of ~ 3 mm. Each tube was cut to a length of 70 mm and subsequently coated with Al and Ti using pack cementation. The pack mixture consisted of 57 wt pct Al_2O_3 powder (filler), 30 wt pct Ti powder (source), 10 wt pct Raney Ni precursor powder (Ni-50 wt pct Al, source), and 3 wt pct NH_4Cl powder (activator), as used in prior studies[15] of pack cementation of woven Ni-20Cr wires. The braid and the pack mixture were placed in an alumina crucible, which was then inserted in the water-cooled end of a tube furnace preheated to 1000 °C. The crucible remained at the water-cooled end for 15 minutes while the furnace was flushed with Ar, and it was then slowly pushed into the hot zone of the furnace. After holding for a specified duration (15, 30, or 60 minutes), it was pulled back to the water-cooled end where it remained for 15 minutes to cool. After cleaning in an ultrasonic bath with acetone to remove all powders remaining on the wires, the as-coated samples were encapsulated in quartz tubes under vacuum. The heat treatment consists of four steps: (1) TLP bonding (1130 °C/1 hour), (2) homogenization (1100 °C/24 hours), (3) solutionizing (1200 °C/2 hours), and (4) aging (900 °C/12 hours for the 30-minute coated samples and 900 °C/24 hours for the 60-minute coated samples). The first three steps were continuous and the samples were water quenched at the end of the solutionizing and aging steps. The samples were then prepared using standard metallographic techniques for optical microscopy and scanning electron microscopy (SEM). Compositions were measured using energy-dispersive X-ray spectroscopy (EDS). The mechanical properties were evaluated *via* tensile tests at room temperature using a loading rate of 10 N s^{-1}. Sample architecture was examined *via* X-ray tomography using

NICOLAS LIPPITZ is with the Institute for Materials, TU Braunschweig, Langer Kamp 8, 38106 Braunschweig, Germany. Contact email: n.lippitz@tu-braunschweig.de DINC ERDENIZ and DAVID C. DUNAND are with the Department of Materials Science and Engineering, Northwestern University, 2220 Campus Drive, Evanston, IL 60208. KEITH W. SHARP is with TexTech Industries, Inc., 1 City Center, Portland, ME 04101.

Manuscript submitted October 27, 2017.
Article published online January 18, 2018

a "Nanotom S" device from General Electric (Wunstorf, Germany); to achieve a high spatial resolution, multiple section scans, covering the full width of the braided tubes, were carried out along the longitudinal axis and then merged into a single reconstruction. With this technique, a voxel size of 5.5 μm was reached. The same sample was imaged after each strain step: the first two steps accumulated 1 pct total strain (elastic and plastic) each, and the following steps accumulated 1.3 pct total strain each, resulting in an average plastic deformation of ~ 0.8 pct for each step.

Optical micrographs of wire contact zones for coating times of 15, 30, and 60 minutes are shown in Figures 1(a) through (c). The bonds are created in the solid-state during pack cementation and enabled by the growth and eventual contact of the wires due to Al and Ti deposition during the coating process. This resulted in relatively small bonding areas with sharp cusps for 15 minutes of coating, as also observed with wire-woven structures.[15] As described in a previous study, the coating consists of three layers: (1) an outer Ni_2AlTi layer, (2) an intermediate $Ni_3(Al,Ti)$ layer, and (3) an inner Cr-rejection layer, with Cr precipitates in the γ'-matrix.[15] The bonded areas between wires are growing with the coating time increasing from 30 to 60 minutes, and they also exhibit relatively smoother cusps. This is due to the deposition of larger amounts of Al and Ti, which increases the wire diameters. As the wires grow, the gaps between neighboring wires close, resulting in an increased number of bonds or bonds with larger areas. Also, during this longer coating period, there is more time for surface diffusion, which explains the smoother cusps. The weight gains achieved due to Al and Ti deposition for 15-, 30-, and 60-minute coating times are 3.8, 4.8, and 6.2 wt pct, respectively. The weight gains achieved for 30 and 60 minutes of coating at 1000 °C are similar to the weight gains observed for 3-D woven structures.[15] The 3-D braided parts subjected to 30- and 60-minute coating times were selected for TLP bonding and heat treatment for the creation of a γ/γ' microstructure.

The bonded and fully heat-treated cross section exhibited in Figure 1(d) shows an extensive bonding area formed by the creation of a TLP, as described for the 3-D woven structures in Reference 15. SEM images of a sample that was alumino-titanized for 60 minutes and fully heat treated is shown in Figure 2. The images show a higher volume fraction of γ'-precipitates in the bonding regions than in the centers of the wires. This is due to a gradient in Al and Ti, the γ' forming elements, concentrations from the bonding regions to the center of the wires, as observed in EDS scans. For the samples that were coated for 30 minutes, the Al concentration decreased from 1.2 to 0.8 wt pct from the bonding region to the center of the wire and the Ti concentration decreased from 3.6 to 1.6 wt pct. As observed in a previous study, a γ' microstructure, similar to the one seen in the bonding regions, requires Al and Ti

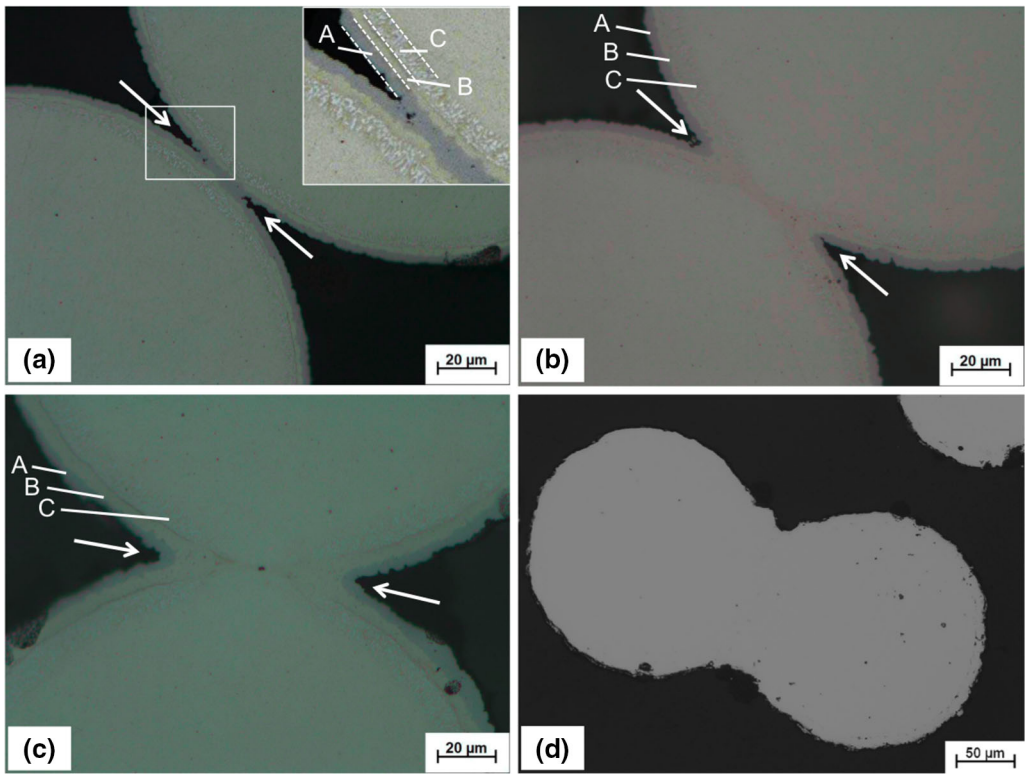

Fig. 1—Optical micrographs of the cross sections of bonded wire pairs after alumino-titanizing by pack cementation for (*a*) 15 min, (*b*) 30 min, and (*c*) 60 min, showing increasing bonding area and cusp radii (arrows) and increasing coating thickness (A: Ni_2AlTi, B: $Ni_3(Al,Ti)$, and C: Rejected Cr in γ). (*d*) Pair of wires after a full heat treatment (alumino-titanized for 60 min, TLP-bonding and homogenization, solutionizing and aging), showing increased bonding area and disappearance of the coating layers seen in (a) through (c).

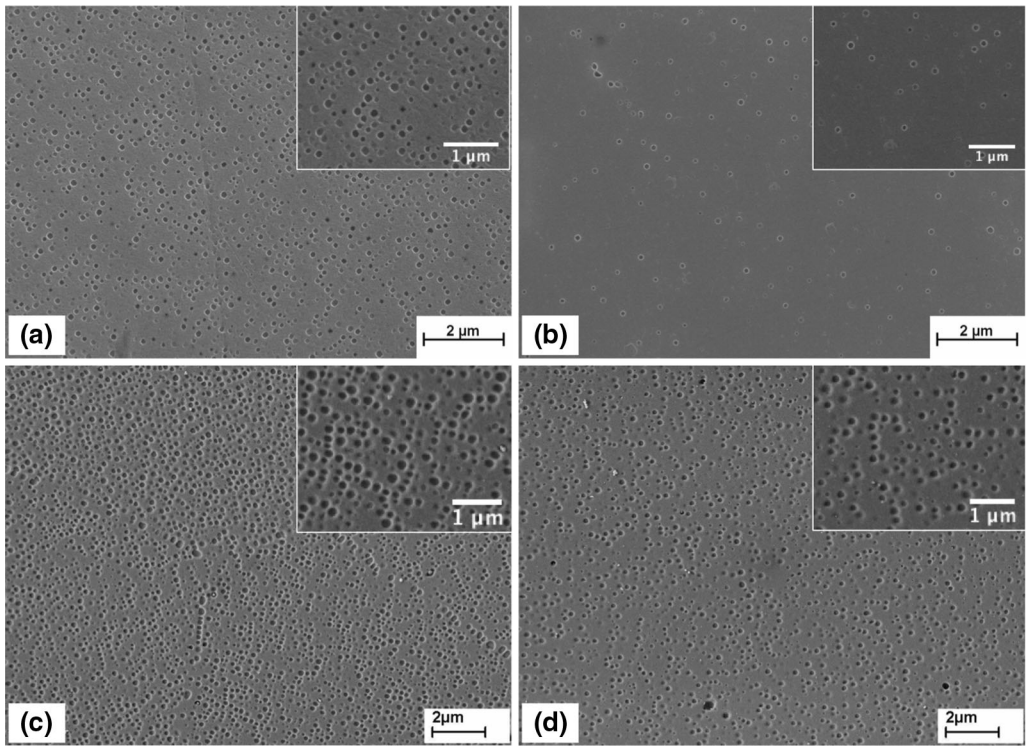

Fig. 2—SEM micrographs of cross sections showing a γ/γ' microstructure for fully heat-treated samples. (*a*) Bonding region after coating for 30 min, (*b*) center of a wire after coating for 30 min, (*c*) bonding region after coating for 60 min, and (*d*) center of a wire after coating for 60 min. Insets show the γ/γ' microstructure at higher magnification.

concentrations of about 1 and 3 wt pct, respectively.[15] To reach a sufficient concentration of both Al and Ti, the samples were coated for 60 minutes instead of 30 minutes. This resulted in mean Al and Ti concentrations at the wire centers (as averaged over five wires per sample) of 1.1 and 2.8 wt pct, respectively. For the bonding regions, the Al and Ti concentrations were 1.5 and 4.4 wt pct, respectively. As expected, the increased coating time results in a higher volume fraction of γ' precipitates in the bonding regions than the centers of the wires.[8,15] Even though the difference in γ' volume fraction for the bonding regions and the center of the wires for the samples coated for 60 minutes is not as apparent as for the those coated for 30 minutes, there are still more γ' precipitates in the bonding regions (compare Figures 2(c) and (d)). The effects of a lower γ'-volume fraction in the center of the wires are also confirmed by microhardness measurements. For the center of the wires and the bonding regions, mean hardnesses of 335 and 403 HV were achieved, respectively. This gradient in composition can be avoided by increasing the homogenization time, but at the risk of losing Al by evaporation. However, a more highly alloyed and, thus, stronger bonding region where stress concentration occurs may, in fact, be desirable. Modeling and failure analysis could shed light on whether a concentration gradient is desirable.

The samples used for the tensile tests exhibited an average weight gain of 3.5 wt pct after 60 minutes of alumino-titanizing, as opposed to 6.2 wt pct for the samples used for metallography. The lower weight gain is related to the design of the grips of the tensile test samples. To prevent crushing of the braided tubes in the grip regions, two cylindrical stainless steel cores (marked with "C" in Figure 3), with the length of the grip, were inserted into the tubes before coating (shown in Figure 3(a)). This might have affected the final composition in two possible ways: (1) the stainless steel inserts might have reduced the gas flow through the braids or (2) some of the Al and Ti might have deposited onto the insert, acting as a sink. Nevertheless, EDS analyses revealed that the Al and Ti concentrations were sufficiently high to achieve the formation of a γ-γ' microstructure. To improve gripping, two stainless steel tube halves were glued to the ends of the braided tubes (marked with "T" in Figure 3) to transfer the tensile load more equally to all wires.

The results of the tensile tests are shown in Figure 4. The stresses refer to the load divided by the sum of the cross-sectional areas of the wires, obtained from the tomographic images. One sample was tested in the as-braided, unalloyed condition (red curve) and three samples in the alloyed and aged condition (black curves). The alloying of the braided tubes and the heat treatment described previously lead to higher tensile strengths due to precipitation-hardening effects of the γ/γ' microstructure. One of the braided superalloy tubes shows a tensile strength similar to that of the as-braided, unalloyed material. Any difference in γ'-volume fraction or microhardness was not observed between these samples. Therefore, premature failure was probably caused by sample-to-sample variation in bonding

between wires. The fracture strain of the superalloy braids is lower than that of the as-woven braids, because bonding between wires prevented them from rotating in the loading direction and, thus, limited the elongation of the braids. This effect also causes a stiffening of the braided superalloy tubes, as observed during handling of the braids and in the stress-strain curves.

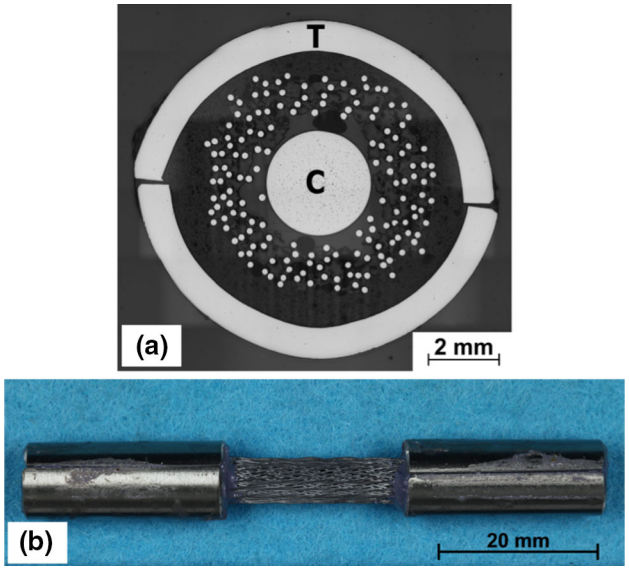

Fig. 3—Tensile test sample with grips: (*a*) cross section of the grip with steel core (marked with "C") and half tubes (marked with "T") and (*b*) sample showing gage and grip sections.

One of the braided superalloy tubes was subjected to an interrupted tensile test (dashed lines), in combination with computed tomography (CT) scans, so that damage could be observed and initial failure locations could be detected. This particular sample was scanned before the interrupted tensile test, to create a reference, and at defined tensile strains, to examine the porous structure, similar to the procedure described in Reference 17. The CT images in Figure 4 show the failure location close to the core that was inserted to create the grip, for the reference condition before the tensile test and after applied strains of $\varepsilon = 7.3$ and 9.1 pct. Braid failure starts with the fracture of a few individual wires, which leads to a flattening of the stress-strain curve; accumulation of wire fractures ensues, terminated by a 50 pct drop in stress. Although the majority of the wires fractured during the test, a few remained intact, holding the sample together. All fractures occurred between the bonding regions, while the bonds remained intact. This is consistent with the microstructural images and microhardness measurements, showing more γ' precipitates and higher hardness values for the bonding regions. Also, all braided superalloy tubes broke in the gage section, close to the grip. At that location, the braids

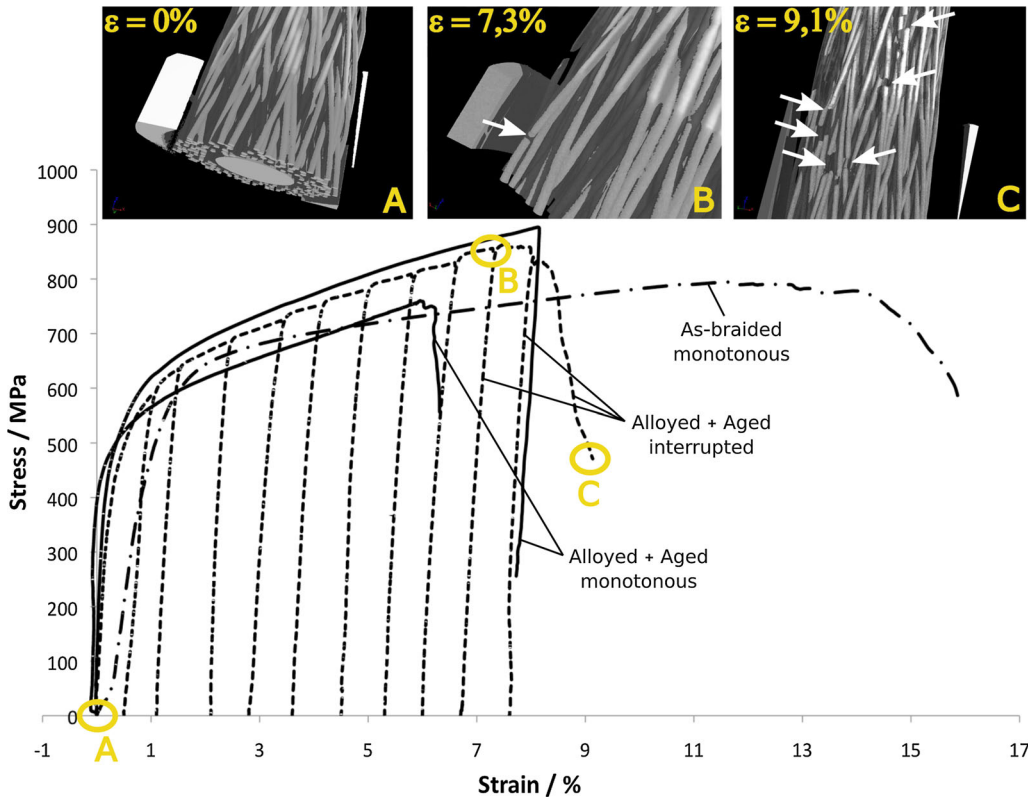

Fig. 4—Tensile stress-strain curves for one as-braided, unalloyed sample and three alloyed, fully heat-treated samples. Tomographic images of the interrupted tensile tests (dashed lines) show the failure region near the grip for tensile strains of (*a*) 0 pct, (*b*) 7.3 pct, and (*c*) 9.1 pct, with wire fracture shown with arrows. A single wire has a diameter of 202 μm.

were probably weakened by reactions of the Ni-20Cr wires with the stainless steel core, which was inserted before the coating process. EDS measurements indeed revealed an Fe content of up to 12 wt pct in wires close to the inserted stainless steel core. Also, the microhardness values are significantly lower for wires close to the core, reaching only 288 HV in the center of the wires and 341 HV for the bonding regions. Due to this experimental artifact, the tensile strength values measured here do not represent the full potential of the braided superalloy tubes.

We demonstrated that tubes braided from ductile Ni-20Cr wires can be transformed into superalloy compositions *via* gas-phase alloying and a subsequent heat treatment that forms a γ/γ' microstructure as well as bonding between the wires *via* the formation of a TLP. Due to the bonding between wires and precipitation hardening, both the stiffness and the tensile strength of the braided structures increased. Interrupted tensile tests and X-ray tomographic imaging identified the regions close to the grips as failure initiation sites, due to the reactions between the steel grip cores and the braided wires. To obtain true mechanical properties, a large series of tensile tests with an improved grip design are required. Also, the failure within the wires was away from the wire bonding areas, indicating a strong and ductile bond, as a result of higher Ti and Al contents and higher γ'-volume fraction compared to wire cores. If a uniform γ-γ' microstructure for all wire regions is desired, longer homogenization times are needed.

The authors acknowledge financial support from the Defense Advanced Research Projects Agency under Award No. W91CRB-10-1-0004 (Dr. Judah Goldwasser, program manager). NL thanks the Sonderforschungsbereich 880, Deutsche Forschungsgemeinschaft, and its graduate research program, Modul Graduiertenkolleg (MGK), for the financial support. Special thanks to Professor Joachim Rösler, the Institute for Materials–TU Braunschweig, for helpful discussions and comments. This work made use of the OMM Facility, which receives support from the MRSEC Program (NSF DMR-1121262) of the Materials Research Center at Northwestern University, and the EPIC facility of the NUANCE Center at Northwestern University, which has received support from the Soft and Hybrid Nanotechnology Experimental (SHyNE) Resource (NSF NNCI-1542205); the MRSEC program (NSF DMR-1121262) at the Materials Research Center; the International Institute for Nanotechnology (IIN); the Keck Foundation; and the State of Illinois, through the IIN.

REFERENCES

1. J. Banhart: *Progr. Mater. Sci.*, 2001, vol. 46, pp. 559–632.
2. A.G. Evans, J.W. Hutchinson, N.A. Fleck, M.F. Ashby, and H.N.G. Wadley: *Progr. Mater. Sci.*, 2001, vol. 46, pp. 309–27.
3. H.N.G. Wadley, N.A. Fleck, and A.G. Evans: *Compos. Sci. Technol.*, 2003, vol. 63, pp. 2331–43.
4. H.N.G. Wadley: *Philos. Trans. R. Soc. A*, 2006, vol. 364, pp. 31–68.
5. B. Hinze, J. Rosler, and N. Lippitz: *Metals*, 2012, vol. 2, pp. 195–201.
6. T.A. Schaedler, A.J. Jacobsen, A. Torrents, A.E. Sorensen, J. Lian, J.R. Greer, L. Valdevit, and W.B. Carter: *Science*, 2011, vol. 334, pp. 962–65.
7. K. Sharp, D. Mungalov, and J. Brown: *Procedia Mater. Sci.*, 2014, vol. 4, pp. 15–20.
8. D. Erdeniz, A.J. Levinson, K.W. Sharp, D.J. Rowenhorst, R.W. Fonda, and D.C. Dunand: *Metall. Mater. Trans. A*, 2015, vol. 46A, pp. 426–38.
9. J.-H. Lim and K.-J. Kang: *Mater. Trans.*, 2006, vol. 47, pp. 2154–60.
10. Y.-H. Lee, B.-K. Lee, I. Jeon, and K.-J. Kang: *Acta Mater.*, 2007, vol. 55, pp. 6084–94.
11. L. Zhao, S. Ha, K.W. Sharp, A.B. Geltmacher, R.W. Fonda, A.H. Kinsey, Y. Zhang, S.M. Ryan, D. Erdeniz, D.C. Dunand, K.J. Hemker, J.K. Guest, and T.P. Weihs: *Acta Mater.*, 2014, vol. 81, pp. 326–36.
12. Y. Zhang, S. Ha, K. Sharp, J.K. Guest, T.P. Weihs, and K.J. Hemker: *Mater. Des.*, 2015, vol. 85, pp. 743–51.
13. L.Y. Zhao, S.M. Ryan, J.K. Ortega, S. Ha, K.W. Sharp, J.K. Guest, K.J. Hemker, and T.P. Weihs: *Int. J. Heat Mass Transf.*, 2016, vol. 96, pp. 296–311.
14. A.J. Levinson, D.J. Rowenhorst, K.W. Sharp, S.M. Ryan, K.J. Hemker, and R.W. Fonda: *Mater. Charact.*, 2017, vol. 124, pp. 241–49.
15. D. Erdeniz, K.W. Sharp, and D.C. Dunand: *Scripta Mater.*, 2015, vol. 108, pp. 60–63.
16. D. Erdeniz, T.A. Schaedler, and D.C. Dunand: *Scripta Mater.*, 2017, vol. 138, pp. 28–31.
17. N. Lippitz and J. Rosler: *Metals*, 2015, vol. 5, pp. 591–602.